Measurements of the infrared emissivity of a wind-roughened sea surface

Jennifer A. Hanafin and Peter J. Minnett

Spectral statistical-analysis techniques were developed and applied to high-spectral-resolution infrared measurements of the sea surface. The effective incidence angle of a ship-borne instrument in typical at-sea conditions was found to introduce errors of up to 0.7 K in sea-surface temperature retrievals at a 55° view angle. The sea-surface emissivity was determined over the 8–12-μm window at view angles of 40° and 55° and at wind speeds up to 13 ms^{-1}. The emissivity was found to increase in magnitude with increasing wind speed, rather than decrease, as predicted by widely used parameterizations. Use of these parameterizations can cause significant bias in remote sensing of sea-surface temperature in noncalm conditions.

OCIS codes: 010.4450, 010.7340, 120.6660, 120.0280, 240.6690.

1. Introduction

The oceans play a pivotal role in the global circulation system by storing heat absorbed at low latitudes and redistributing it to higher latitudes. Most of the heat subsequently released to the atmosphere is transferred through the sea surface by sensible and latent heat fluxes and thermal radiation. This energy source is significant for atmospheric circulation on short[1] and long[2] temporal scales and spatially from meso scale[3,4] to large scale.[5] Sea-surface temperature (SST) is used as both a prognostic and diagnostic variable in numerical weather prediction and in global climate modeling. Satellite-derived SST fields with an absolute accuracy of better than 0.3 K are required for large time- or space-scale studies of global atmospheric circulation.[2,6] This level of accuracy may also be necessary to determine the ocean's part in the global carbon cycle, a further requirement for accurate climate predictions; Van Scoy *et al.*[7] estimated a significant mean increase in global ocean CO_2 drawdown (0.39 Gt C yr^{-1}) when the sea-surface cool-skin effect is taken into account.

In order to make accurate SST retrievals from satellite, air-borne, or ship-based radiometers, the sea-surface emissivity (ϵ) must be known. Emissivity is the ratio of the thermal radiation emitted by a body to that from a perfect blackbody, and it is wavelength (λ) and emission angle (θ) dependent for most materials. The radiometric measurement of SST is very sensitive to this parameter: a 1% change in ϵ corresponds to a change in retrieved SST of 0.66 K (at $\lambda = 10$ μm), 0.73 K (at $\lambda = 12$ μm), or 0.24 K (at $\lambda = 3.5$ μm). So, to reach the SST measurement accuracy required for climate research, ϵ must be known to $<0.5\%$ in the 8–12-μm wavelength region, and $<1\%$ in the 3–4.5-μm window. An outstanding gap in our knowledge is how wind and waves roughening the sea surface affect ϵ. Compared with a flat water surface, a wavy sea surface has an increased surface area and, when viewed from a fixed pointing angle, has significant and time-dependent angular perturbations of the local surface. This study assesses the effect of sea-surface roughness on ϵ and its effect on measurements of SST from sensors deployed on ships, in particular, where ship pitch and roll also cause perturbations in instrument pointing angle.

When wind blows over a water surface, a capillary wave field is produced almost immediately. The surface wave field changes with wind speed, fetch, and wave age,[8] however, and the topography of a patch of ocean is the result of the instantaneous wind and the long waves produced by the wind at a distance (swell). Wind speed can be used as a proxy for sea-surface roughness, therefore, and theoretical studies such as that of Masuda *et al.*[9] (hereinafter referred to

When this research was performed, the authors were with the Division of Meteorology and Physical Oceanography, Rosenstiel School of Marine and Atmospheric Science, University of Miami, Virginia Key, Florida 33149. J. A. Hanafin (j.hanafin@imperial.ac.uk) is now with Space and Atmospheric Physics, Imperial College London, South Kensington, SW7 2BZ, UK.

Received 4 March 2004; revised manuscript received 20 August 2004; accepted 21 September 2004.

0003-6935/05/030398-14$15.00/0

as the Masuda model) have parameterized ϵ as a function of wind speed, by modeling the geometry of the sea surface in terms of wind-speed-dependent distributions of facets and slopes. The Masuda model is widely used in SST retrieval algorithms; however, evidence from observational work by Watts *et al.*[10] (hereinafter referred to as the Watts model) indicates that the model overestimates the wind-speed dependence of ϵ. This study corroborates this evidence, presenting measurements from two research cruises that show ϵ increasing with increasing wind speed, rather than decreasing as predicted by the Masuda model.

High-resolution spectral measurements, such as from the marine–atmosphere emitted radiance interferometer[11] (M-AERI), are particularly appropriate for conducting studies of spectral emissivity, $\epsilon(\lambda)$, of natural surfaces. Smith *et al.*[12] outlined a technique for determining $\epsilon(\lambda)$ of water from field data. The $\epsilon(\lambda)$ of water is a smooth function of wavelength, whereas high-spectral-resolution radiation measurements of water taken in the field contain the signatures of numerous atmospheric emission lines resulting from the reflection of sky radiation. By a process of iteration, the reflectivity of the surface can be determined by minimizing the correlation between the sky radiation and the spectral emissivity. In this study, a similar approach with different methodology was used to find the effective incidence (or emission) angle of the measurements, and then Fresnel's equations were used to determine the emissivity of the surface.

2. Data

A. Instrumentation

The M-AERI is a well calibrated, Fourier-transform infrared (IR) interferometer.[11] It is a passive instrument, which measures the radiance emitted by both the sea surface and the atmosphere at complementary angles (Fig. 1). Each sequence of scene views is sandwiched between two calibration sequences consisting of measurements of the emission from two blackbody cavities and known temperature, one at ambient air temperature and the other much warmer (60 °C). Radiance measurements are averaged over 1–3-min intervals. The measured emitted radiance spectra (W m^{-2} Sr^{-1} cm^{-1}) are in the wavenumber (υ) range 500–3000 cm^{-1} (approximately 3–20 μm; see Fig. 2 for a sample of the data) and have a spectral resolution of 0.5 cm^{-1}. The accuracy of the derived brightness temperatures in this wavelength region has been determined to be <0.02 K at 20 °C and <0.04 K at 30 °C.[11]

B. Determination of the Emissivity of Water from a Stable Platform

To test the statistical techniques used in this study, an experiment was carried out on the grounds of the Rosenstiel School of Marine and Atmospheric Sciences, University of Miami, where measurements of the emissivity of a smooth water surface over a range of water temperatures were made. A M-AERI was deployed, measuring the radiance emitted from an open bath of heated fresh water with a path length of ~0.7 m. The water in the tank was heated to 40 °C; then measurements were made every 8–9 min as the water cooled down to ambient air temperature. The water was then cooled by ~7 °C, and measurements were made as the water warmed up.

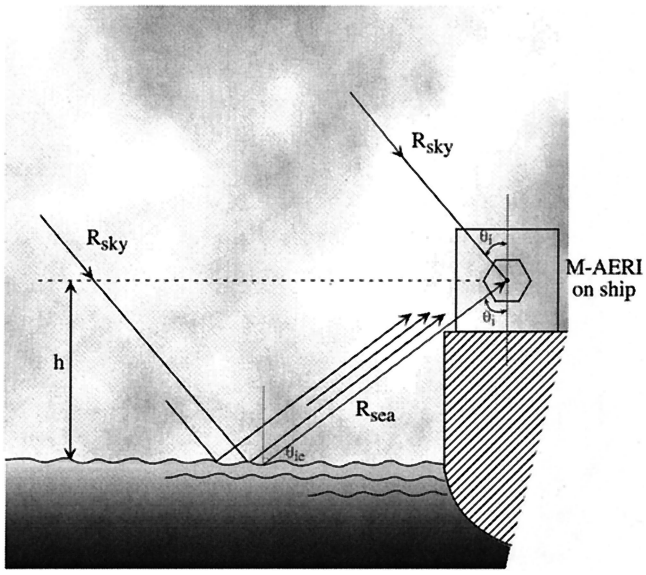

Fig. 1. Schematic of M-AERI viewing geometry on a typical deployment at sea. The sea and sky radiances, R, are measured from a height, h, with an instrument pointing angle of θ_i and an effective incidence angle of θ_{ie} at the sea surface.

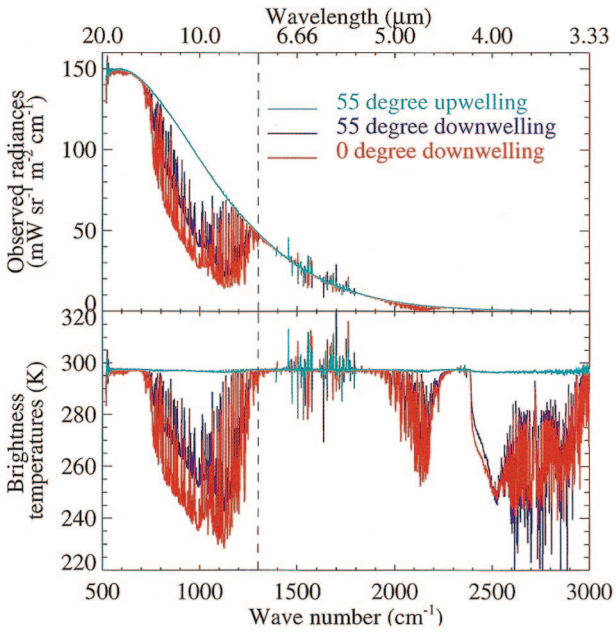

Fig. 2. Sample of M-AERI radiance data (upper panel) and its equivalent brightness temperature (BT) (lower panel). Atmospheric window regions are evident, as sky BT is colder in these regions, with warmer spikes corresponding to absorption and emission by atmospheric gases.

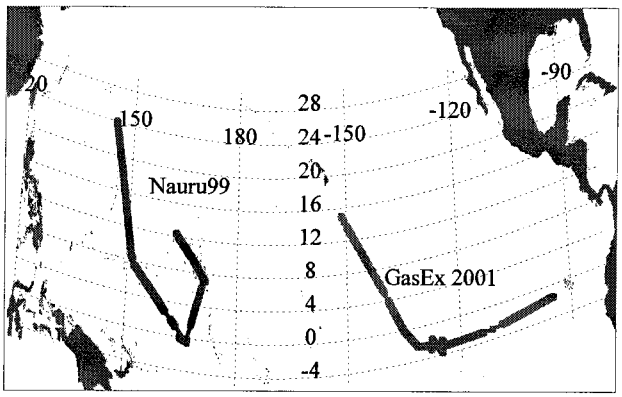

Fig. 3. Cruise tracks for Nauru99 and GasEx 2001.

C. Field Campaigns

Data from two cruises were analyzed, Nauru99 and Gas Exchange (GasEx) 2001; see Fig. 3 for cruise tracks. The Nauru99 experiment, conducted in the tropical western Pacific ocean in June and July 1999, was a joint project among the Department of Energy's Atmospheric Radiation Measurement program, the National Oceanographic and Atmospheric Administration, and the Japan Marine Science and Technology Center. The RV *Mirai* left Yokohama, Japan, on 5 June and steamed south to Nauru. The intensive observation period (IOP) took place in the vicinity of Nauru from 17 June to 4 July. During the IOP, the vessel had a regular 3-h schedule, steaming slowly into the wind for 1 h for eddy correlation flux measurements, then steaming back to the original position and staying on station for an hour. The IOP was characterized by fair weather with light to moderate winds ($<10\ \mathrm{ms}^{-1}$). Air temperatures ranged from 26.2–28.2 °C and SSTs from 28.0–29.3 °C. The M-AERI was on a platform 6 m above the main deck, looking slightly forward to avoid the bow wave at a pointing angle of 55°. After the IOP, the ship steamed northeast. Data were collected until 9 July.

GasEx 2001 had very similar conditions to Nauru99, but was located in the tropical eastern Pacific Ocean. The M-AERI was installed on the O2 deck of the RV *Ronald H. Brown*, with a pointing angle of 55° to starboard. Data collection began on 7 February 2001, when the *Ronald H. Brown* was just south of the equator and steaming westward to the first IOP at 3° S, 125° W on 14 February. The second IOP was at 2° S, 130° W on 22 February. Both IOPs involved a series of 3–12-h stations, in a grid of 1° × 1° latitude, so there is a series of transits and stations. Whenever possible, the ship steamed slowly into the wind for eddy correlation measurements. On 1 March, the *Ronald H. Brown* began steaming northwest, and data collection ceased on 7 March. Data used here are from yeardays 38 to 48 and 58 to 66.

Only nighttime data (19:30–06:30 h) with clear skies were included in the analysis. Daytime data were not used, to avoid the possibility of undetected contamination of the measurements by sunlight entering the instrument, either directly or by reflection at the sea surface. The cruise tracks are shown in Fig. 3, and statistics for each cruise are given in terms of variable ranges, means, and number of data points that were used in analysis in Table 1. The data used were strictly quality controlled. The techniques described in the next section to determine the spectral emissivity rely on atmospheric absorption features being reflected at the sea surface, which are masked by low and mid-level clouds. Clear-sky data only were analyzed, and ceilometer data were used to confirm the absence of clouds. Measurements taken when the relative wind may have been carrying air contaminated by the ship's smoke stack were discarded. Those retrieved during turning maneuvers were also removed from analysis, as the measured downwelling radiance would not necessarily coincide geometrically with the measured upwelling radiances in these cases.

D. Refractive Index of Water

The reflectivity of a medium can be determined from its refractive index and the incidence angle, using Fresnel's equations. Knowledge of the refractive index is necessary to retrieve the incidence angle using the variance-minimization technique (VarMinT) described in the following section. A detailed review and evaluation of the refractive index of pure and sea water and its temperature and solute dependence currently available in the literature were carried out before this analysis.[13] The main absorption features in the IR water spectrum are the v_2 bending mode of the H_2O molecule ($1640\ \mathrm{cm}^{-1}$), the librational peak frequency ($570\ \mathrm{cm}^{-1}$), and a satellite component of the bending band ($2120\ \mathrm{cm}^{-1}$).[14] When validating the analysis techniques used here,

Table 1. Summary of Statistics of Meteorological Variables during Nauru99 and GasEx 2001 Field Campaigns

	Nauru99 (N = 117)			GasEx 2001 (N = 341)		
	Min	Max	Mean	Min	Max	Mean
Air temperature (°C)	26.2	28.2	27.3	23.2	26.7	25.1
Sea-surface temperature (°C)	28.0	29.3	28.5	24.1	27.0	25.4
Wind speed (ms^{-1})	0.3	8.9	4.1	0.5	15.1	4.7
Air pressure (mbar)	1008	1014	1011	1007	1015	1009
Relative humidity (%)	65	82	72	63	94	87

significant differences were found between published refractive-index data for pure water. The data reported by Bertie and Lan[15] were produced using the average of imaginary refractive-index spectra obtained using a Circle (manufactured) multiple attenuated-total-reflection cell by four different researchers over 7 yr. The real part of the refractive index was determined using Kramers–Kronig analysis with improved techniques. Citing a critical review of the techniques used and the results of their own work and of other studies, they recommended the optimal values for different wavelength regions. These data gave the best results in the validation exercise and were used in the subsequent analysis when required.

Changing the temperature of a water molecule can affect both the intensity (strength) and the frequency of absorption features, thus changing the refractive index. Pinkley *et al.*[14] measured the ratio of reflectance of 27 °C water to water of temperatures between 1 °C and 50 °C. Most significant for SST remote-sensing applications is the spectral nonlinearity of the temperature dependence of reflectance from 800–1200 cm^{-1}. While there is a small region around 1100 cm^{-1} that shows no dependence, above and below this region there is a variability of up to 1% per °C in reflectance of water between 16 °C and 39 °C. The results of Pinkley *et al.*[14] were used to correct for this temperature dependence.

The difference between the reflective properties of pure water and artificial seawater or salt solutions has been investigated by Pinkley and Williams,[16] who determined the relative reflectance for a standard seawater solution[17] at near-normal incidence angles. As with the temperature dependence, the 8–12-μm window is most affected by typical seawater solute concentrations.

A spectral region that is sensitive to angular changes, but not to temperature or solute changes, was required to determine the effective incidence angle of the measurements with the VarMinT. The magnitude of the refractive index of water is sensitive to temperature throughout the spectrum, however, and the frequency of absorption peaks also changes with temperature and concentration of solute present. So, although the 8–12-μm region is very sensitive to incidence angle, its sensitivity to changes in temperature or salt content render it unsuitable for this type of analysis until these dependencies are more fully and accurately characterized. The 2130–2190-cm^{-1} region (4.5–4.6 μm) was chosen, as water reflectivity is sensitive to changes in angle around the 55° instrument pointing angle used here (for comparison, at viewing angles of 40°, the sensitivity of emissivity to a change in angle is only 25% that at 55°). The spectral variation of reflectance with changing temperature or solutes is small across this spectral region, although a satellite absorption band centered nearby (2120 cm^{-1}) undergoes a slight frequency shift to lower frequencies with temperature.[14]

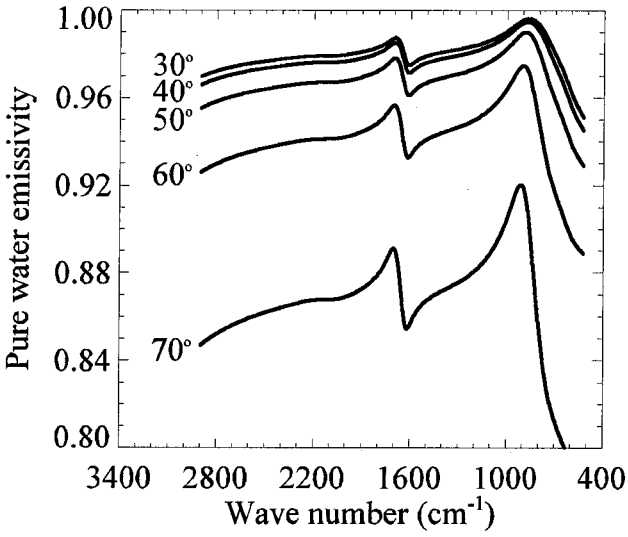

Fig. 4. Angular dependence of emissivity across the IR spectrum calculated from Fresnel equations using refractive-index data[15] for incidence angles of 30°–70°.

3. Method

A. Spectral Brightness Temperature Variance-Minimization Technique to Determine the Effective Incidence Angle

To retrieve the brightness temperature (BT) of the sea surface, its blackbody equivalent radiance, $R\uparrow$, must be found using

$$R(\lambda) = \epsilon(\lambda)R\uparrow(\lambda) + \rho(\lambda)R\downarrow(\lambda), \tag{1}$$

where R is the measured upwelling radiance, $R\downarrow$ is downwelling sky radiance (see Fig. 1), and ρ is the sea-surface reflectivity. All of the quantities are wavelength dependent. The atmospheric transmissivity between the instrument and the sea surface is here assumed to be 1, as the path length between the instrument and the sea surface is so short, ~10 m for a typical sea-going deployment and ~0.7 m for determination of the emissivity of water from a stable platform (DEWS), and the wavelength regions used have high atmospheric transmissivity.

The spectral reflectivity of the sea surface, ρ, was computed from the parallel and perpendicular polarization components, $\rho_\parallel$ and $\rho_\perp$, using Fresnel's equations in the form

$$\begin{aligned}
\rho &= (\rho_\perp + \rho_\parallel)/2, \\
\rho_\parallel &= r_\parallel{}^2 = \left(\frac{n_t \cos\theta_i - n_i \cos\theta_t}{n_i \cos\theta_i + n_t \cos\theta_t}\right)^2, \\
\rho_\perp &= r_\perp{}^2 = \left(\frac{n_i \cos\theta_i - n_t \cos\theta_t}{n_i \cos\theta_i + n_t \cos\theta_t}\right)^2,
\end{aligned} \tag{2}$$

where θ_i and θ_t are the incidence and transmission angles, and n_i and n_t are the refractive indices of air and water. The wavelength and incidence-angle dependence for ρ is shown in Fig. 4.

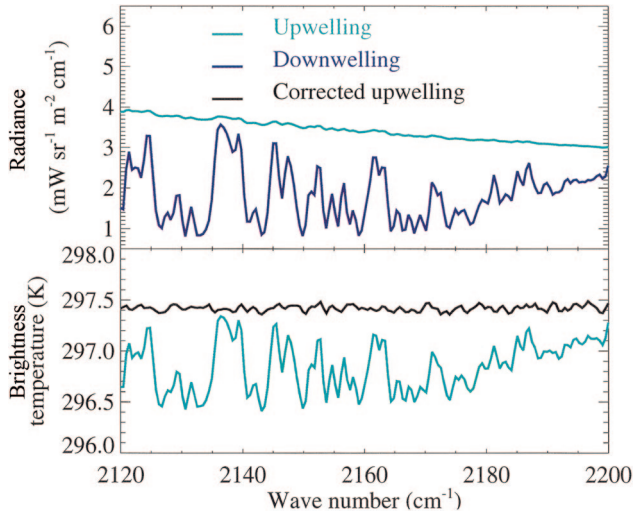

Fig. 5. Sample of M-AERI radiance and corresponding BT showing high degree of correlation between upwelling uncorrected BT and downwelling radiance and reduction of BT variance from ±0.5 K to ±0.05 K when the correction for reflected radiance is applied.

As these data were measured from a ship, both its motion and any waves on the surface will change the effective incidence angle (θ_{ie}) of the measurements. The spectral resolution of the M-AERI is high enough to resolve many individual absorption features in the spectra. These features are visible in the upwelling radiance spectra as a result of reflection at the sea surface of the atmospheric emission (Fig. 5) and are also visible in the brightness spectra derived from these radiances. When the ideal atmospheric correction is made, the absorption features disappear in the brightness-temperature spectrum. To find this correction, the reflectivity was calculated at different incidence angles until the variance of the brightness temperature across the spectral region was minimized. This is shown in the next subsection to be a robust technique for determining the effective incidence angle of ship-borne radiometric data, when due care and attention is paid to the choice of spectral region and refractive-index data are used.

B. Linear VarMinT to Determine Sea-Surface Emissivity

The technique described in Wu and Smith[18] begins by inverting Eq. (2) to get an expression for ϵ:

$$\epsilon = \frac{R_{\mathrm{OBS}}\uparrow - R_{\mathrm{OBS}}\downarrow}{R_{\mathrm{SEA}}\uparrow - R_{\mathrm{OBS}}\downarrow}, \tag{3}$$

where R_h is assumed negligible in the window region. The underlying assumptions are that downwelling sky radiance is not correlated with $\epsilon(\lambda)$ and that $\epsilon(\lambda)$ is a spectrally smooth function. This technique uses refractive-index data to compute the spectral emissivity, however, and the uncertainty in the refractive index of seawater is a source of error that was avoided here by using a piecewise linear VarMinT approach.

The data processing using this technique is similar to that described above, but the variance minimization is over small wavenumber ranges (<10 cm^{-1} in the 8–12-μm region), and the emissivity is assumed to be constant over these ranges. Rearranging Eq. (3) to give an expression for the BT of the sea surface with emissivity as the only unknown,

$$BT_{\mathrm{SEA}} = B^{-1}\left[\frac{R_{\mathrm{OBS}}\uparrow - (1-\epsilon)R_{\mathrm{OBS}}\downarrow}{\epsilon}\right]. \tag{4}$$

The emissivity value corresponding to the mean Fresnel value at θ_{ie} across the wavenumber range was taken as a first guess. This numeric value was then incrementally changed until the BT variance across that wavenumber segment was minimized.

The technique described in the previous subsection was applied to the data over different wavenumber ranges, and the results were binned in 10-cm^{-1} ranges. A digital low-pass filter was then applied to the spectrally binned average to produce a smooth spectral emissivity without altering the peak frequency through boxcar smoothing.

4. Results

A. Evaluating Technique Performance

The DEWS experiment was designed to test the performance of the techniques described above under controlled conditions. The aims were the following:

to evaluate and compare the different refractive-index data available and determine which should be used in application of the VarMinT to at-sea measurements;
to verify reproducibility and evaluate accuracy of both the VarMinT and the linear VarMinT; and
to investigate any temperature dependence in the results of both techniques.

Four different refractive-index data sets were compared: Pontier and Dechambenoy,[19] Segelstein,[20] Wieliczka *et al.*,[21] and Bertie and Lan.[15] Knowing that $\theta \approx 55°$, the VarMinT was carried out on each data set, and the computed θ_{ie} was compared (Fig. 6). As each of the refractive-index data sets was measured at different temperatures from 25–35 °C, the results of Pinkley *et al.*[14] were used to correct for the difference between the SST (T_S) and the refractive-index reference temperature (T_R). This study[14] measured the spectral reflectance of water at four different temperatures relative to that at 27 °C and found an almost linear relationship with temperature across the spectral range 2000–2400 cm^{-1}. A correction factor[13] based on these results was applied to the Fresnel reflectivity (ρ) to calculate the temperature-corrected reflectivity (ρ_T): $\rho_T = [1 - 0.00174(T_S - T_R)]\rho$.

The accuracy of the M-AERI brightness-temperature measurement is ±0.03 K between 20 and 30 °C, so, from Table 2, the accuracy limit of the incidence angle retrieval in the 3.5–5-μm region is ±0.5°. Another factor in determining the limits of

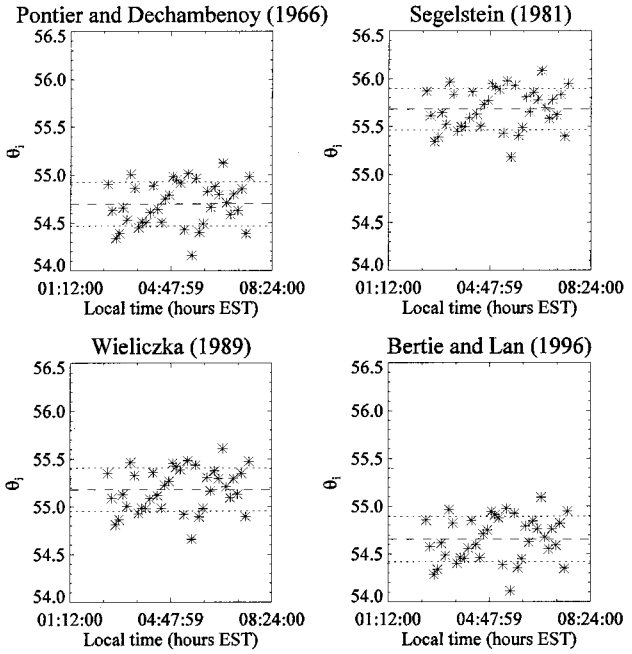

Fig. 6. Comparison of the capability of different published refractive-index data to predict θ_{ie} for a calm water surface on a stable platform at an instrument pointing angle of 55°. The dashed curve indicates the mean, and the dotted curve is the variance.

accuracy of this technique is the accuracy of the refractive-index data. The errors as estimated by Bertie and Lan[15] were shown to be negligible in reflectivity space at these frequencies.[13]

The results of the comparison are listed in Table 3. Changing the refractive-index data that was used only changed significantly the magnitude of the computed θ_{ie}, having no effect on its variance. The mean of every data set tested was within the pointing angle plus or minus the limit of the technique, except for that of Segelstein,[20] which is 0.7° from the pointing angle. While the mean for the data of Wieliczka *et al.*[21] is closest to 55°, no reference temperature was reported for those data, so they were rejected from further consideration. The results using data from Pontier and Dechambenoy[19] and Bertie and Lan[15] are indistinguishable, considering the 0.5° limitation of the technique at these frequencies, so that of Bertie and Lan[15] was chosen, as they are likely to have benefitted from technological advances and the experience of research carried out in the previous 30 years. These refractive-index data were used throughout the remaining analyses, with the temperature and seawater reflectance corrections from Pinkley *et al.*[14] and Pinkley and Williams[16] used when necessary.

Table 2. Sensitivity of Retrieved BT to θ_{ie} and ϵ at 55° and 40° Incidence Angles and Water Temperature of 295 K

Angle	Wavelength (μm)	$d\epsilon/d\theta_{ie}$ (%/°)	$dBT/d\epsilon$ (K/%)	$dBT/d\theta_{ie}$ (K/°)
55°	3.6	−0.26	−0.242	0.063
	10.8	−0.13	−0.66	0.087
	12.0	−0.19	−0.731	0.14
40°	3.6	−0.054	−0.237	0.013
	10.8	−0.021	−0.651	0.014
	12.0	−0.026	−0.717	0.019

To determine the temperature dependence of the results, the correlation between the computed θ_{ie} and T_S was computed. θ_{ie} did not show any dependence on T_S in the 20–40 °C range of the experiment, in this frequency range (correlation coefficient of 0.01). When the technique suggested by Smith *et al.*[12] was used to analyze the same data, θ_{ie} showed a difference of $-0.55°$ over the same temperature range. This corresponds to a change in reflectivity of 0.00174 K^{-1}, which is that predicted by relative reflectance measurements of Pinkley *et al.*[14] in this wavenumber region. The VarMinT implicitly corrects for temperature dependences, removing this potential error source from the results.

The errors appear to be normally distributed about the mean ($\theta = 54.64°$, $N = 38$), and 63% of the computed θ_{ie} were within one standard deviation (0.22°) of the mean. 97% were within two standard deviations (±0.45°), which is just under the instrument accuracy limit, showing that the VarMinT is robust and capable of determining incidence angles to within ±0.5°, in the 2130–2190-cm^{-1} wavenumber range.

The spectral water-surface emissivity calculated using the linear-piecewise method is plotted in Fig. 7(a) with the emissivity calculated using Bertie and Lan[15] plotted as a dashed black curve for comparison. The spectral shape of the measured emissivity is very similar to that of the predicted, but its magnitude is less than predicted below 1000 cm^{-1} by 0.5% at 900 cm^{-1} and by up to 1.5% at 800 cm^{-1}. The same tendency was noted by Wu and Smith[18] at wavenumbers below 900 cm^{-1}.

Also, this is a persistent feature in the results of both fresh and seawater measurements (see below), and the relative reflectances measured here for different temperatures [Fig. 7(b)] and for fresh and salt water (Fig. 8) compare very well with those measured by Pinkley *et al.*[14] and Pinkley and Williams.[16] As noted above, this frequency region is sensitive to both temperature and solutes. While the magnitude of the difference cannot be ascribed to the fairly small temperature dependence at these wavenumbers, the presence of dissolved or surfactant materials could be a factor. These results may represent the emissivity of a monomolecular surfactant layer rather than that of the water alone. It should be noted that refractive-index studies make a great effort to keep the water and water surface as clean as possible. No such effort was made during DEWS, making the results more representative of natural water-surface emissivity than data from pure water. Furthermore, larger errors are expected in the refractive-index data for this spectral region for all measurement techniques.[15]

Table 3. Results of Refractive-Index Comparison Using DEWS Data

	Pontier and Dechambenoy[19]	Segelstein[20]	Wieliczka *et al.*[21]	Bertie and Lan[15]
Mean θ_{ie} ± std. dev.	54.7° ± 0.05	55.7° ± 0.05	55.2° ± 0.05	54.6° ± 0.05

The emissivity was measured at different temperatures, from 20–40 °C, and the relative reflectances agree substantially with those of Pinkley *et al.*[14] The emissivities were averaged in 5 °C temperature bins [Fig. 7(a)], the reflectivity calculated, and the ratio of the reflectivities of the 22.5 °C (dark blue), 32.5 °C (yellow), and 37.5 °C (red) to the 27.5 °C (green) reflectivity is shown in Fig. 7(b). The magnitude of the reflectivity decreases with temperature throughout this wavenumber region. There is very little change with temperature in the 900–1100-cm^{-1} region, but a larger effect is visible from 800 to 900 cm^{-1} and from 1100 to 1200 cm^{-1}. The values around 800 and 1200 cm^{-1} have larger errors associated with them, as atmospheric absorption begins to become nonnegligible in the radiative transfer at and beyond these frequencies.

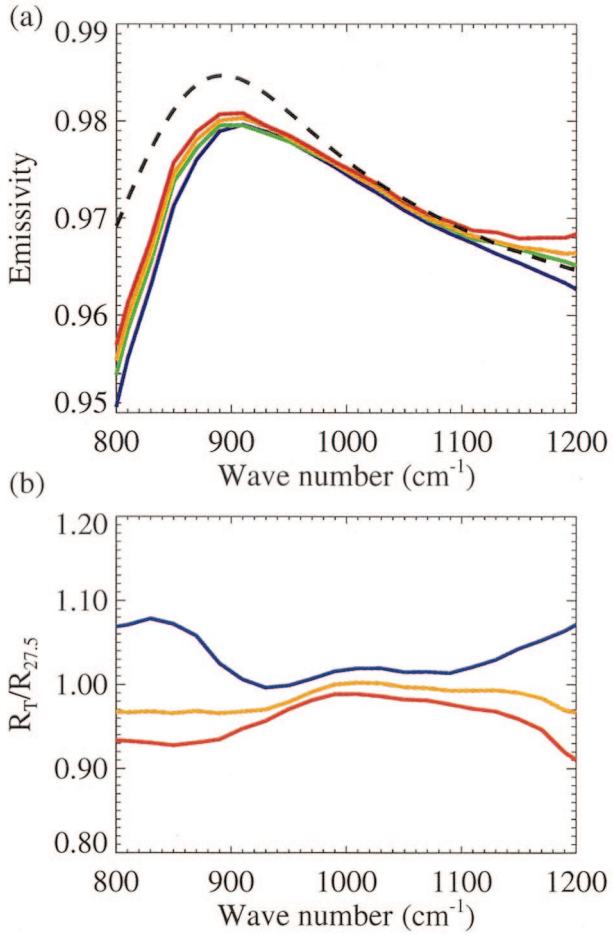

Fig. 7. Measurements of water-surface spectral emissivity. (a) The emissivity was averaged in 5 K bins, centered on 22.5 °C (dark blue), 27.5 °C (green), 32.5 °C (yellow), and 37.5 °C (red). The dashed curve shows the emissivity predicted from Fresnel equations and the refractive index of water.[15] (b) Ratio of measured reflectances of 22.5 °C, 32.5 °C, and 37.5 °C water to 27.5 °C water.

B. Effective Incidence Angle of a Sea-Going Radiometer

Figure 9 shows the time series of θ_{ie} determined using the VarMinT for Nauru99 and GasEx 2001. The instrument pointing angle was 55° in each case, and the mean θ_{ie} of both data sets falls within 0.8° of this nominal incidence angle. The variance of the Nauru99 data is 0.65 (Table 4), which is within 30% of the ±0.5° instrumental accuracy as previously determined. The variance of the GasEx data is larger, as the data were collected under a larger range of meteorological conditions. The "calm condition" mean θ_{ie} is closer to 56° (see Fig. 10). This discrepancy from the nominal pointing angle is considered acceptable, as the instrument was leveled with a liquid level on a ship moored to a dock, and fuel or ballast water added or removed asymmetrically across the vessel would affect the actual pointing angle.

Histograms of the θ_{ie} are plotted in Fig. 11 and display negative skewness. This skewness was not a feature of the DEWS data, and it can be attributed to the influence of waves in the field of view. While the effect of ship motion should, in general, be symmetric around the pointing angle, a wave field will, on average, act to reduce the incidence angle. The emission from the waves facing toward the instrument will be sampled preferentially for two reasons. First, the emissivity is inversely related to the incidence angle, so as the wave facets tilt toward the instrument, reducing the emission angle, more energy is emitted

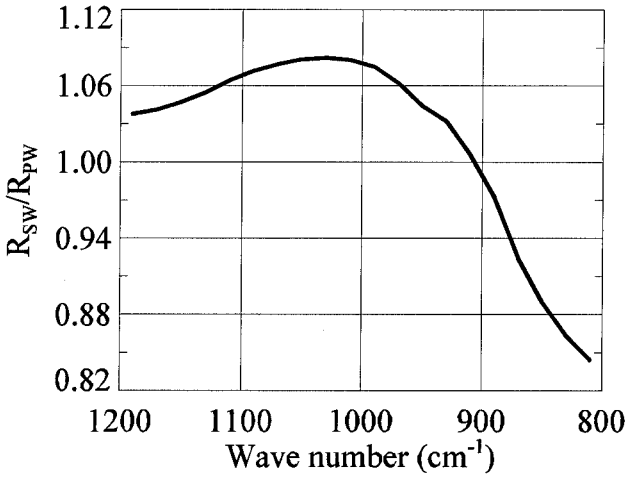

Fig. 8. Reflectance ratio of mean 56° (calm condition mean θ_{ie}) spectral sea-surface reflectivity/DEWS spectral fresh-water reflectivity.

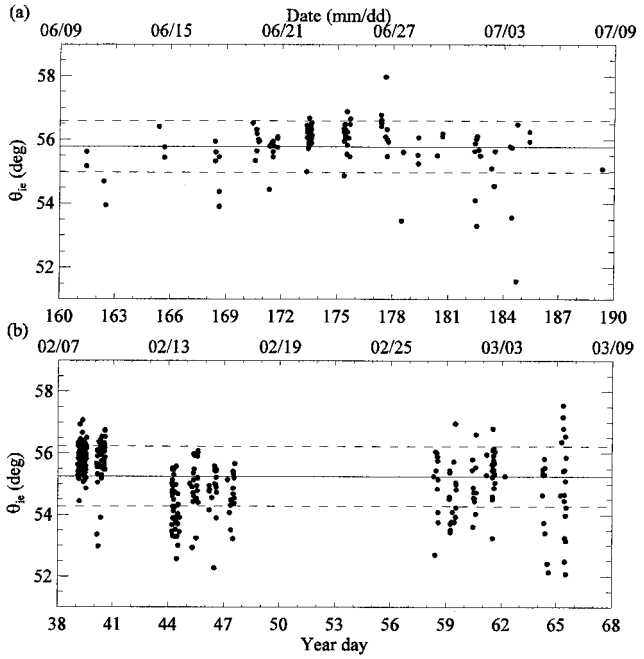

Fig. 9. Time series of θ_{ie} computed for Nauru99 and GasEx 2001. The mean is plotted as a solid line and the variance as a dashed line.

in the beam reaching the instrument. Second, the waves themselves block some of the radiance emitted from wave troughs and slope angled away from the instrument, particularly at higher incidence angles, even if there is a secondary-reflection mechanism.[10]

While ship motion will cause a symmetric change in incidence angle, waves will cause θ_{ie} to be negatively skewed. As both of these factors depend to first order on wind speed, it is of interest to determine the behavior of the θ_{ie} at different wind speeds. Figure 10 shows θ_{ie} as a function of wind speed. The trend is for the magnitude of θ_{ie} to decrease with wind speed. The scatter is very small in calm conditions (<3 ms^{-1}) but increases up to ± 3–$4°$ of pointing angle as the wind increases. In fact, a slight increase in the range around 3–4 ms^{-1} could be due to capillary waves enhancing the surface roughness. This would affect the measurements in two ways: by increasing the mean slope of the wave field, or by the enhanced roughness affecting the validity of the bidirectional reflectance assumption. The second possibility is ruled out by use of the BT variance across the spectrum as a quality-control parameter, as it is an indicator of how well the technique performs, large BT variance indicates a poor match between the reflected upwelling and downwelling radiances. Also, there

Table 4. Statistics of θ_{ie} as Measured on Two Field Campaigns

Campaign	Mean θ_{ie}	Variance θ_{ie}	N	Min θ_{ie}	Max θ_{ie}
GasEx 01	55.25	0.96	341	52.08	57.55
Nauru99	55.78	0.65	116	51.57	57.98

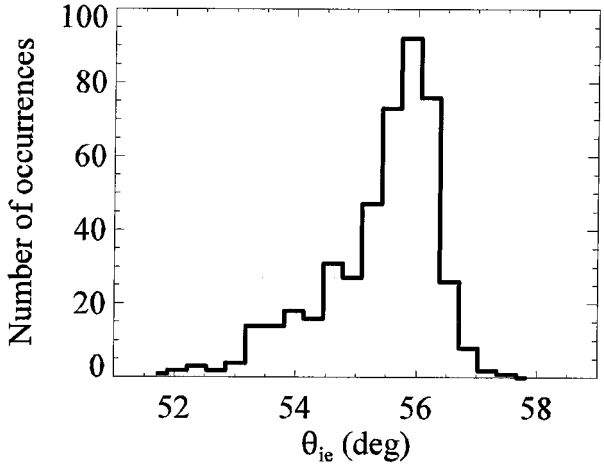

Fig. 10. Histogram of θ_{ie} for Nauru99 and GasEx 2001, showing negative skewness.

was no apparent correlation between BT variance and wind speed in the remaining data.

C. Sea-Surface Spectral Emissivity

The results of the linear VarMinT are presented in Fig. 12. The emissivity computed for an incidence angle of 55° using refractive-index data from Bertie and Lan[15] is plotted as a dashed black curve. The computed emissivities compare well with the predicted values over most of the 800–1200-cm^{-1} range. Values at either end of the range have larger discrepancies, particularly around 1150–1200 cm^{-1} as atmospheric absorption becomes more important in the radiative transfer. This is more obvious in the Nauru99 data, as the path length of the instrument was slightly longer than for the GasEx 2001 configuration. The range of emissivity is about 1% over this entire frequency range, which is twice the accuracy required for the stated SST retrieval accuracy.

In order to examine the features of the emissivity as determined by the piecewise linear VarMinT, the numerical values at 910 and 1110 cm^{-1} (± 10 cm^{-1})

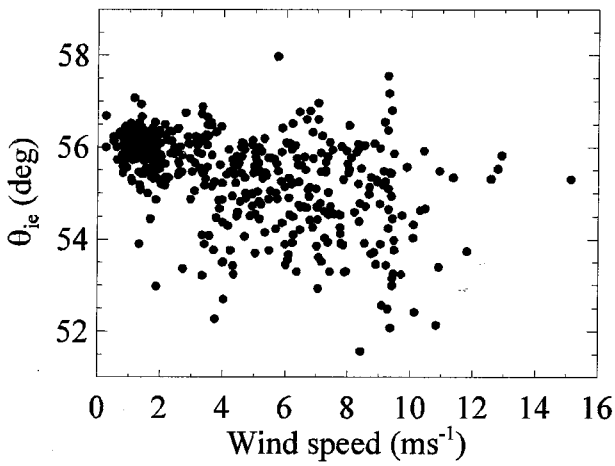

Fig. 11. Scatter plot of θ_{ie} with wind speed.

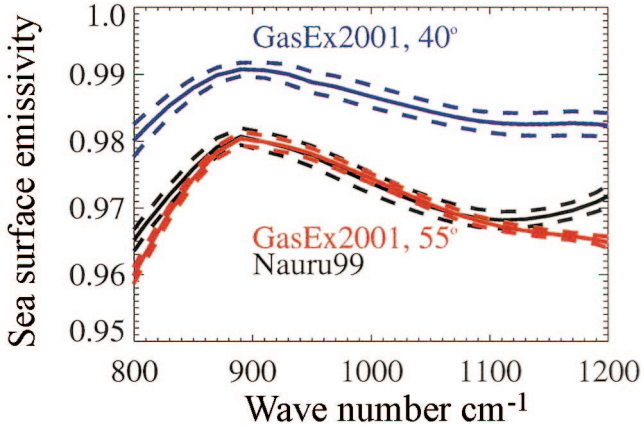

Fig. 12. Spectral sea-surface emissivity from 800–1200 cm^{-1} (12.5–8.33 μm) computed using a piecewise linear variance minimization technique from GasEx 2001 data at viewing angles of 55° and 40° and Nauru99 data at a 55° view angle. The standard deviations are plotted as a dashed curve.

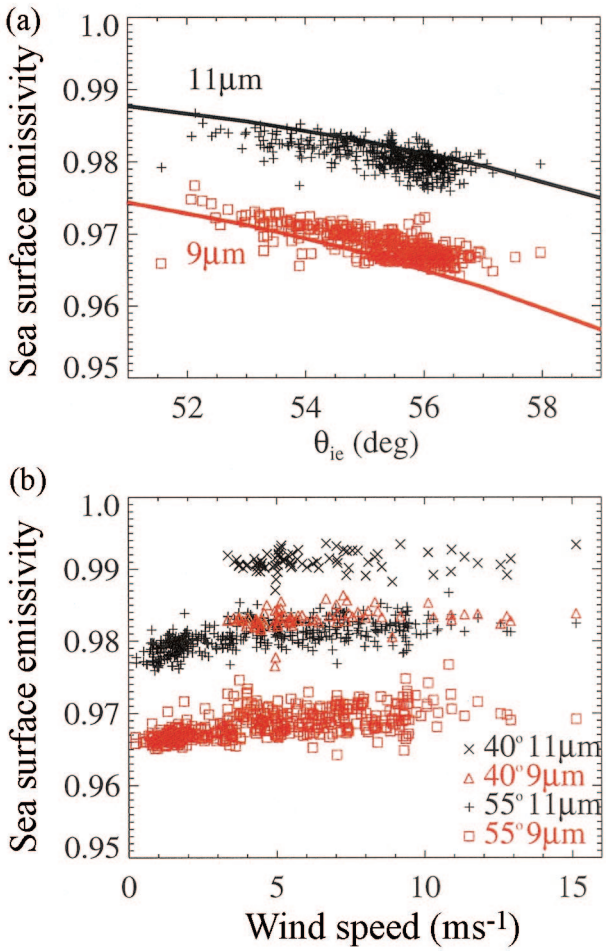

Fig. 13. Nauru99 and GasEx 2001 55° measured 910- and 1100-cm^{-1} emissivity values plotted (a) as a function of retrieved effective incidence angle θ_{ie} and (b) sea-surface emissivity from 40° and 55° instrument pointing angles as a function of wind speed.

were plotted. The numerical emissivity values collapse in θ_{ie} space, with a curvilinear trend [the curve can be determined from the Fresnel equations; predicted values are plotted as lines in Fig. 13 (a)]. This translates into an increase in emissivity with wind speed, rather than the decrease predicted by the Masuda model. This result and implications are discussed in more detail below.

During GasEx 2001, the sequence of data collection varied slightly for the last week to include 40° as well as 55° views. Table 2 shows that the emissivity at a 40° incidence angle is much less sensitive to small angular changes, and the VarMinT was found to be too insensitive to changing incidence angle for determining θ_{ie} in the 2140–2190-cm^{-1} wavenumber range. However, the piecewise linear approach may still be used to determine the spectral emissivity. The 40° spectral emissivity is also plotted in Fig. 12, with the envelope of one standard deviation plotted as dashed curves.

The faster than predicted drop-off of spectral emissivity below 900 cm^{-1} seen in the DEWS fresh-water results and observed by Wu and Smith[18] for a limited set of seawater data, was also observed in these data collected during both Nauru99 and GasEx 2001. As a test of internal consistency, the spectral emissivities computed were analyzed to compare them with the results of Pinkley *et al.*[14] and Pinkley and Williams.[16] To investigate temperature effects, the DEWS data were binned into 5 °C bins, and the reflectance ratio of each temperature bin was compared with the 27.5 °C bin. To compare the reflectance ratio of seawater to fresh water, the spectral emissivities retrieved using the linear VarMinT for cruise data with incidence angles in the range 56° ± 0.5° were averaged in 20-cm^{-1} bins and compared with the mean of the DEWS spectral emissivities (mean water temperature of 303.4 K). The results compare very well with Pinkley and Williams,[16] in magnitude and wavenumber dependence. The ratio increases from 1.05 at 1150 cm^{-1} to about 1.08 at 1030 cm^{-1}, then falls off rapidly, reaching 1.0 at 900 cm^{-1} and continuing to decrease steadily until 800 cm^{-1}. The fall-off below 900 cm^{-1} is slightly larger in these data than reported by Pinkley and Williams,[16] but this region has already been seen to be more sensitive to any deviations from the case of pure 27 °C water.

A possible source of error apart from temperature and solutes in this spectral region could be due to a polarization sensitivity of the instrument. Unfortunately, no measurements have been made to investigate such sensitivity for the particular instruments used in this study. Recently, however, a BOMEM MR100 Fourier-transform infrared interferometer, which is similar to that used in the M-AERI instruments, was found to be 5% sensitive to vertically polarized radiation.[22] This sensitivity becomes an issue for the type of analysis reported here when the source radiation is significantly polarized. A number of factors influence the net degree of polarization reaching a water-viewing sensor, as discussed by Shaw in a series of papers.[22–24] One of these[23] showed that the degree of polarization reaching a water-

viewing sensor at 10-m height under a clear 1976 U.S. Standard Atmosphere model is slightly negatively polarized and varies spectrally for nonnormal incidence angles. The degree of polarization was determined to be at a minimum of $\sim 2\%$ near 9000 cm^{-1} and rising to 4% at 1200 cm^{-1} for a 60° incidence angle. These values are reduced to $<1.5\%$ at these wavelengths for tropical atmospheres, however.

The retrieved sea-surface BT error that was due to -5% instrument polarization sensitivity calculated for the 10-m sensor under a standard atmosphere[22] was found to be -0.06 K at 12 μm and -0.035 K at 10.8 μm for a 60° incidence angle. A rough estimate of the effect on the emissivity retrieved here can be found by working back from the retrieval sensitivities given in Table 2, using these levels of BT error. The negative error implies that if the instrument is more sensitive to vertically polarized radiance, the emissivity is underestimated, by 0.1% at 12 μm and by 0.05% at 10.8 μm. These represent worst-case scenarios, as the degree of polarization at a 55° incidence angle is less than that at 60°, and most of these data were measured under a tropical atmosphere, which reduces the degree of polarization even further.[23]

Although this represents a bias in the right direction, it is an order of magnitude lower than required to compensate for the differences between the retrieved emissivities and those calculated from refractive-index data. With regard to the effective incidence angle, the BT error reported from that study[22] is less than instrument accuracy at the wavelengths used for the retrieval; however, it would represent a maximum bias of approximately $-0.3°$. Until the polarization sensitivity of the instruments used here and the degree of polarization of the source have been confirmed, however, these biases belong in the error budget for these retrievals.

The level of internal consistency in the results, therefore, points to an environmental cause for the drop-off below 900 cm^{-1}, possibly owing to surfactants. A study by Salisbury and D'Aria[25] found that the spectral signature of oil slicks is almost uniform at these frequencies. Unfortunately, no data on the spectral emission of natural oceanic surfactants in the IR were found in published literature.

5. Discussion

A. Effective Incidence Angle of Ship-Borne Measurements

The possible effects of a difference between an instrument pointing angle and the actual incidence angle of ship-borne radiometric measurements have been estimated by a recent study.[26] The retrieval of the effective incidence angle presented here allows the magnitude of the effect of ship motion and wave action on T_S retrievals to be determined. This is a heretofore unknown element of the error budget of radiometric SST retrievals, and, as the results presented here show, can be significant at larger view angles.

The effect of a change in incidence angle on SST retrievals is twofold, affecting both the upwelling component through the emissivity and the reflected downwelling component through the reflectivity of the sea surface. From Fig. 9, the combined effects of ship motion and wave action have a net effect of up to 6.4° on the range of the effective measurement angle over an averaging period of 45–60 s and a spatial average of ~ 10 cm^2. These averaging intervals are fairly typical for ship-borne radiometric measurements. A 3°–4° difference between nominal and actual incidence angle corresponds to a T_S error of 0.26–0.35 K at 10.8 μm or 0.42–0.56 K at 12 μm. Even at the less sensitive 3.6 μm, a 4° error in pointing angle corresponds to a 0.25 K error in temperature retrievals, which is more than double the stated (<0.1 K) accuracy of many radiometric measurements.[27,11]

Figure 14 illustrates the different effects of ship and wave motion on θ_{ie}, by plotting the histograms of the lower ($u < 3$ ms^{-1}), moderate (3 $ms^{-1} < u < 8$ ms^{-1}), and higher ($u > 8$ ms^{-1}) wind-speed regimes. In calm seas, the range of θ_{ie} is $\pm 1°$, distributed almost normally with slight negative skewness around the median. This range is due to ship pitch and roll, which is expected to be quite symmetric about a mean position. In moderate winds, the median value decreases by 0.5°, the range of θ_{ie} increases, and more negatively skewed values appear as the wave field begins to play a larger role. At high winds, the spread increases again. The difference between the mean low wind θ_{ie} calculated and the instrument pointing angle is 1°. This could be due to a mean ship tilt, an error in the pointing-angle alignment, or the salt-water correction applied to the pure-water refractive-index data. The relative reflectance used to correct the refractive index[16] was measured at near-normal incidence angles and may have a small angular dependence that would bias the magnitude of θ_{ie} calculated using the VarMinT technique.

These results indicate that the changing incidence angle constitutes a significant component of the error budget of SST retrievals. The effect of ship roll and wave field is generally assumed to average out over the typical spatial and temporal averaging scales of SST measurements. As shown here, however, even in very calm conditions, there is a $\pm 1°$ change in incidence angle owing to either swell or ship roll. At instrument pointing angles $\geq 55°$, this small difference alone can represent the entire desired SST measurement accuracy of 0.1 K. The choice of pointing angle is often determined by the ship's geometry, in order to avoid sampling the "bulk" temperature of water disturbed by the bow wave rather than the undisturbed "skin" temperature, for example. Future measurements of SST can minimize this source of error by using instrument pointing angles closer to nadir whenever circumstances allow. A further recommendation from the discussion of refractive index is to avoid the 8–12-μm region when measuring SST, as its sensitivity to both water temperature and salt

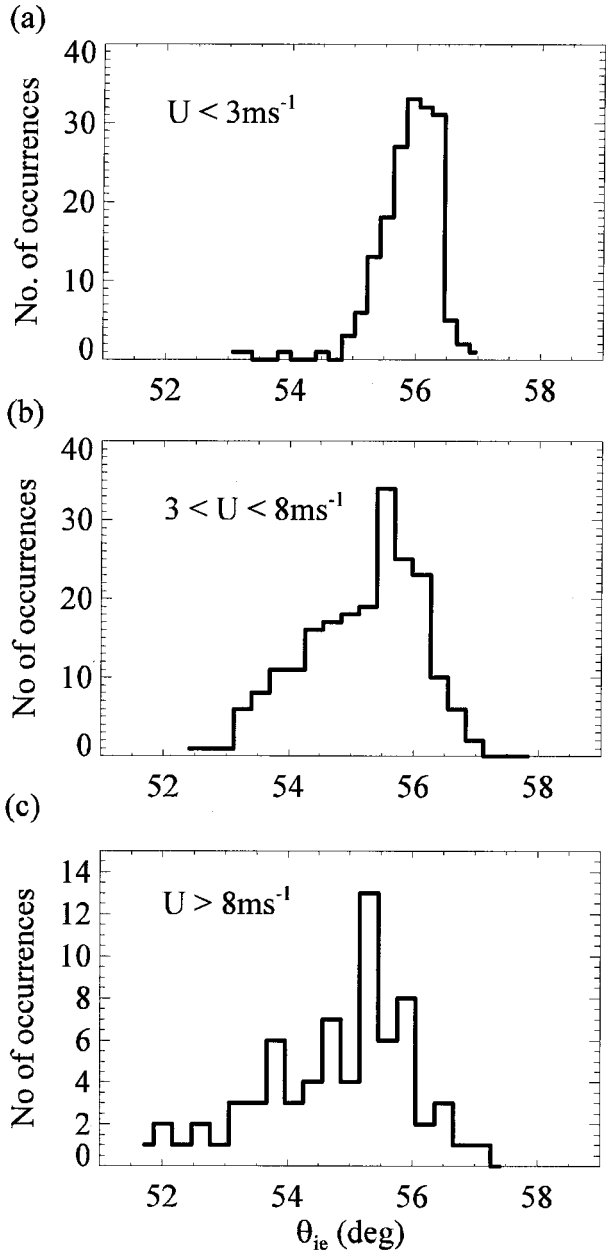

Fig. 14. Histogram of θ_{ie} in (a) low, (b) moderate, and (c) moderate-high wind-speed regimes. The effect of waves becomes apparent in (b) and (c) as a negative skewness and spreading of θ_{ie} away from the median.

and solute content is high and currently not well characterized at these frequencies.

B. Sea-Surface Spectral Emissivity

The separation of temperature and emissivity is an issue in making quantitative temperature retrievals from remote-sensing measurements.[28] The ability to determine the magnitude of the emissivity of the sea surface from field measurements allows determination of the effects of sea-surface roughness on SST retrievals. Second to the refractive index of seawater, the effective angle of incidence is a large factor determining the variability of the effective spectral emissivity of the sea surface. As the wind speed is the single main factor affecting the surface roughness, it has generally been modeled as a wind-speed-dependent function. The results presented here show, however, that the measured sea-surface emissivity has the opposite trend with wind speed to that predicted using these models. Using these models in SST retrievals introduces a bias, which is significant in all but the calmest oceanic conditions.

C. Sea-Surface Emissivity as a Function of Wind Speed: Models versus Observations

Using the Gaussian distribution of sea-surface slope as a function of wind speed from the Sun glitter measurements of Cox and Munk,[29] Takashima and Takayama[30] modeled the rough sea surface as a series of facets and presented the emissivity as a function of wind speed. The complex refractive index of pure water was approximated using the real part only. Published at about the same time was a very similar treatment by Sidran,[31] who used the complex refractive index of pure water from Hale and Querry[32] and included a discussion of polarization of reflected and emitted radiation. Masuda *et al.*[9] developed this model by normalizing with a factor to account for "wave shadowing" of reflected radiation, preventing the modeled emissivity from becoming boundless at large view angles. Again, the complex refractive index of pure water from Hale and Querry[32] was used, but was corrected for seawater using Friedman's[33] formulation in the Masuda model. A further development to this approach was suggested by Watts *et al.*,[10] by including a parameterization of multiple reflections of sea-surface emitted radiation, notably the surface-emitted surface-reflected radiation. This is radiation emitted by the sea surface and reflected at oblique angles from slope facets facing away from the instrument into the measurement direction. It was estimated for different wind speeds using the Masuda model for rough sea-surface emission and typical sea-surface slopes. Addition of this component in the Watts model reduced the wind-speed dependence of the emissivity predicted by the Masuda model. The numerical value of emissivity increased by up to 1.5% at 25-ms^{-1} winds, although there was still a small decrease in emissivity predicted at winds less than 10 ms^{-1}. Wu and Smith[18] found that inclusion of surface-emitted surface-reflected radiation improved the comparison of the model when compared with the calculation of sea-surface emissivity using the technique outlined in Smith *et al.*[12] Different combinations of the real and imaginary parts of the complex refractive index were investigated in Wu and Smith's[18] study, and the combination that best fit the observations was a combination of the real part of Hale and Querry,[32] the imaginary part of Segelstein,[20] and the seawater adjustment formula from Friedman.[33]

By comparing the statistics of wave slopes determined from scanning-laser glint measurements, Shaw and Churnside[34] identified a stability depen-

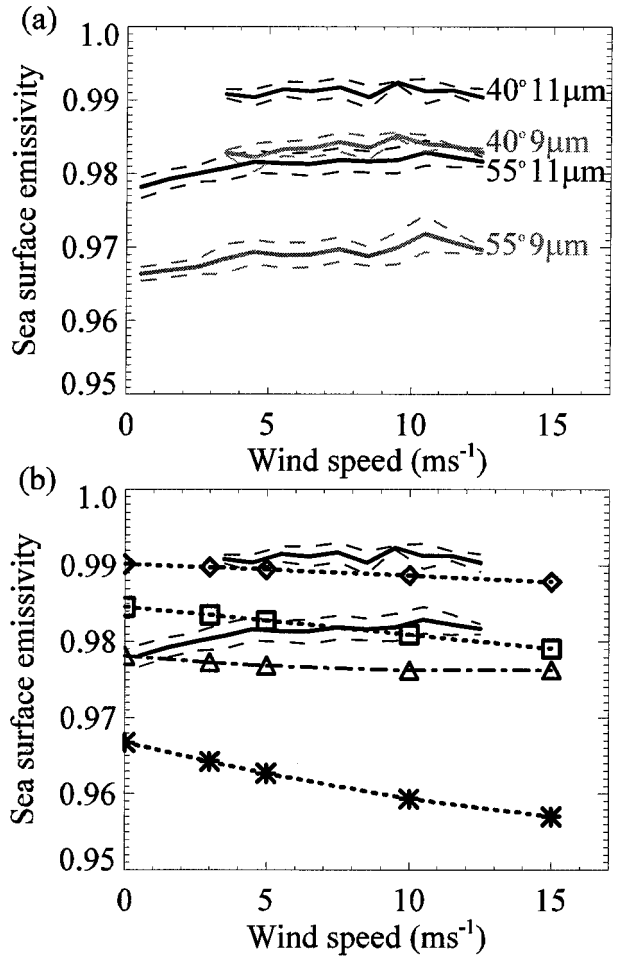

Fig. 15. (a) Observed mean (solid curves) and standard deviation (dashed curves) of sea-surface emissivity in 1 ms^{-1} wind-speed bins for 9 μm and 11 μm at 40° and 55° incidence angles. Values are given in Table 5. (b) Wind-speed dependence of sea-surface emissivity at 11 μm as measured by this study (solid curves) at 40° (upper) and 55° (lower) incidence angles and that predicted by the Watts model (dot-dashed curve) at 52°–55° and the Masuda model (dotted curves) at 40° (◇), 50° (□), and 60° (*).

Table 6. Ratios of 11-μm Reflectivity and Emissivity at Different Incidence Angles

Incidence Angles	Reflectivity Ratio	Emissivity Ratio
40°/25°	1.34	0.998
55°/40°	2.64	0.990
70°/55°	5.16	0.934

dence of sea-surface roughness. Their measurements taken in unstable conditions, with the ocean being warmer than the air, showed a larger mean-square slope when compared with the Cox and Munk[29] measurements, which were taken in neutral and stable conditions. All of the observations used here were taken in conditions of near-neutral and negative stability, with air–sea temperature differences of 0.1 to 1.6 K. The results presented here agree qualitatively with those from the scanning laser, in that a larger mean-square slope means a rougher sea surface and a higher emissivity than indicated by the Cox and Munk[29] results. The data did not, however, show a clear linear dependence with decreasing stability in this regime (see Hanafin[13] for more details) as had been noted by Shaw and Churnside.[34]

The retrieved ϵ at 9 μm and 11 μm from GasEx 2001 data is shown in Fig. 15. These were averaged over 1-ms^{-1} wind-speed bins to produce means and standard deviations for each bin, which are given in Table 5. The trend is for the magnitude of the sea-surface emissivity to increase with wind speed. The results from the Masuda and Watts models are plotted in Fig. 15 for comparison. The solid curves are the measured 11-μm emissivity for the 40° and 55° views; the dashed curve with triangular markers represents values predicted by the Watts model for 55° at 11 μm (the coefficients reported in that paper were valid only for 52°–55° viewing angles). The dotted curves are those predicted by the Masuda model for 40° (diamonds), 50° (squares), and 60° (asterisks).

Table 5. Mean and Standard Deviation of Sea-Surface Emissivity Calculated in 1-ms^{-1} Wind-Speed Bins at 9 μm and 11 μm and 55° and 40° Viewing Angles

	40° Viewing Angle		55° Viewing Angle	
Wind Speed (m/s)	9 μm Mean ± std dev	11 μm Mean ± std dev	9 μm Mean ± std dev	119 μm Mean ± std dev
0–1	–	–	0.96641 ± 0.00091	0.97814 ± 0.00142
1–2	–	–	0.96687 ± 0.00098	0.97923 ± 0.00131
2–3	–	–	0.96737 ± 0.00096	0.98000 ± 0.00117
3–4	0.98288 ± 0.00041	0.99084 ± 0.00061	0.96846 ± 0.00201	0.98073 ± 0.00166
4–5	0.98221 ± 0.00194	0.99037 ± 0.00109	0.96935 ± 0.00161	0.98161 ± 0.00154
5–6	0.98336 ± 0.00090	0.99148 ± 0.00100	0.96892 ± 0.00169	0.98136 ± 0.00133
6–7	0.98346 ± 0.00123	0.99121 ± 0.00126	0.96902 ± 0.00167	0.98131 ± 0.00161
7–8	0.98429 ± 0.00126	0.99172 ± 0.00131	0.96971 ± 0.00167	0.98190 ± 0.00157
8–9	0.98350 ± 0.00164	0.99038 ± 0.00150	0.96880 ± 0.00131	0.98164 ± 0.00144
9–10	0.98523 ± 0.00044	0.99236 ± 0.00026	0.96990 ± 0.00223	0.98186 ± 0.00177
10–11	0.98412 ± 0.00113	0.99122 ± 0.00167	0.97184 ± 0.00249	0.98283 ± 0.00173
11–12	0.98373 ± 2.7E-05	0.99125 ± 0.00061	0.97064 ± 0.00140	0.98225 ± 0.00132
12–13	0.98288 ± 0.00053	0.99040 ± 0.00115	0.96961 ± 0.00048	0.98166 ± 0.00067

When there is no wind, the 55° predicted value of 0.978 is obtained. At 10-ms^{-1} wind speeds, however, the difference between the observed 55° emissivity (0.982) and that predicted by the Watts model (0.976) is equivalent to a -0.4 K difference in retrieved BTs. At a 40° viewing angle, which is less sensitive to wind-speed effects, the values predicted by the Masuda model are offset by approximately -0.003 in the 3–13-ms^{-1} range measured.

The primary mechanism behind the observed increase of emissivity with wind speed is the mean decrease in effective incidence angle that was reported in the previous subsection. For a typical 10-ms^{-1} wind speed, the maximum slope of the waves produced is 15°. Radiance received at an instrument with a pointing angle of 55° from the crests and troughs is emitted at 55°. Radiance received from any other point on the wave is emitted at the instrument pointing angle ±15°. From Table 6, a change of effective incidence angle from 40° to one of 55° increases the emissivity by 1%, whereas a change from 55° to 70° decreases it by 7%. As a result, the radiance reaching the instrument that is emitted from wave facets facing toward it is 1.01 times that from crest/trough facets. The radiance measured from a facet facing away from the instrument is 0.93 times that measured from the normal facets. The nonlinearity of the emissivity angular dependence leads to the radiance reaching the instrument being dominated by that emitted at angles smaller than the instrument pointing angle. At an instrument pointing angle of 40°, the radiance reaching the radiometer is much less sensitive to angular differences: the differences between emission from normal surface facets and those facing toward the instrument ($\theta_{ie} = 25°$) and those facing away ($\theta_{ie} = 55°$) are 0.2% and 1%, respectively.

The change in effective incidence angle of the reflected component offsets that of the emitted component, but is very small. Two factors are at play in the magnitude of the radiation reflected: the increase in reflectivity of the surface with increasing incidence angle, and the angular dependence of the reflected atmospheric radiation field. At facets facing toward the instrument, the incidence angle is smaller, so the radiance reflected has a smaller magnitude, as its atmospheric path length is shorter than that reflected at horizontal facets.

These results substantiate the suggestion of Wu and Smith[18] that at larger incidence angles, the emissivity of the sea surface actually increases as the surface gets rougher, rather than decreases as predicted by commonly used parameterizations.[9,10] The magnitude of the increase with increasing wind speed from 0 to 10 ms^{-1} is ~0.5%. This can be explained by the decrease in the effective incidence angle observed in these data.

6. Conclusions

While the importance of the oceanic skin layer has been recognized in terms of both its role in air–sea interaction and in the remote sensing of SST, the combination of its microscopic scale and the turbulent nature of air–sea boundary layers presents a challenge for field and laboratory experiments. This study addressed issues relevant to IR remote sensing of SST using a combination of new instrumentation, development and refining of analysis techniques, and high-quality laboratory and field measurements. Properties and characteristics of the sea surface, which previously had only been characterized through theoretical approaches, can now be studied using field observations using the techniques described here.

The first quantification of the effect of the changing incidence angle of ship-borne measurements on SST retrievals was presented, and it was found to be up to 6 times the desired accuracy (0.1 K) at a measurement angle of 55° in the IR atmospheric window regions. In general, radiometric SST studies assume that the incidence angle of the measurements is equal to the pointing angle of the instrument. The quantification of this previously unknown error source raises serious questions about SST retrieval error budgets. Analysis of the effective incidence angle of a ship-borne instrument shows that the assumption of a horizontal surface is good to ±1° in calm conditions and up to ±3–4° in wind speeds from 3 to 13 ms^{-1}. For instrument pointing angles of 55° or greater, particularly in the 8–12-μm wavelength range, this angular offset can result in SST errors of up to 0.6 K. The effect is fairly symmetric about the mean in low winds but is skewed toward smaller values of incidence angle at higher wind speeds owing to the tilted facets of the wave field.

Recommendations have been made on the basis of this work for minimization of this source of uncertainty in future studies. Instrument pointing angles of up to 40° are much less sensitive to effects resulting from changes in incidence angle than those >40°. The 8–12-μm window is more sensitive than the 3–5-μm window, and the most significant potential errors are at 11–12 μm. Use of semi-opaque wavelengths for ship-borne remote sensing of SST combined with algorithms that model atmospheric absorption between radiometric instruments and the sea surface are recommended rather than using the very clear atmospheric window regions. The algorithm used to derive skin SST from M-AERI measurements[11,12] uses this approach and is found to be very insensitive to errors caused by changing incidence angle, having a maximum SST error of 40 mK during GasEx 2001.[13]

Further results challenge the validity of widely used models of the response of sea-surface emissivity in the IR to wind roughening. The emissivity of the sea surface was determined without *a priori* knowledge of the refractive index of seawater, which is sensitive to water temperature, salt content, and surfactants, particularly in the 8–12-μm region. This uncertainty in basic data and detailed analysis of the methods used in previous studies[12,18] led to a reassessment of the approach to the rough-water emis-

sivity problem. Following development and evaluation of the analysis techniques, new spectral emissivity results for fresh and seawater were presented. Emissivity measured over a wide range of wind speeds (0 to 13 ms^{-1}) showed a mean increase of 0.004 at a 55° incidence angle and was constant at a 40° incidence angle at wind speeds of 3 to 13 ms^{-1}. This contradicts the predicted trend of a decrease in ϵ with wind speed at all angles. The use of these parameterizations of the wind-speed effect on emissivity can bias SST measurements at high wind speeds by up to 0.4 K.

References

1. L. K. Shay, G. J. Goni, and P. G. Black, "Effects of a warm oceanic feature on Hurricane Opal," Mon. Weather Rev. **128,** 1366–1383 (2000).
2. M. R. Allen, C. T. Mutlow, G. M. C. Blumberg, J. R. Christy, R. T. McNider, and D. T. Llewellyn-Jones, "Global change detection," Nature **370,** 24–25 (1994).
3. L. Eymard, S. Planton, P. Durand, Y. Camus, P. Y. Le Traon, L. Prieur, A. Weill, D. Hauser, B. Le Squere, J. Rolland, J. Pelon, F. Baudin, F. Benech, J. L. Brenguier, G. Caniaux, P. De Mey, E. Dombrowski, A. Druilhet, H. Dupuis, B. Ferret, C. Flamant, P. Flamant, F. Hernandez, D. Jourdan, K. B. Katsaros, D. Lambert, J. M. Lefevre, P. Le Borgne, A. Marsouin, H. Roquet, J. Tournadre, V. Trouillet, and B. Zakardjian, "Study of the air–sea interactions at the mesoscale: the SEMAPHORE experiment," Ann. Geophys. [Paris] **14,** 986–1015 (1996).
4. J. S. Godfrey, R. A. Houze, R. H. Johnson, R. Lukas, J. L. Redelsperger, A. Sumi, and R. Weller, "Coupled ocean–atmosphere response experiment: an interim report," J. Geophys. Res. [Oceans] **103,** 14395–14450 (1998).
5. C. C. Walton, W. G. Pichel, and J. F. Sapper, "The development and operational application of nonlinear algorithms for the measurement of sea surface temperatures with the NOAA polar-orbiting environmental satellites," J. Geophys. Res. **103,** 27999–28012 (1998).
6. I. J. Barton, A. M. Zavody, D. M. O'Brien, D. R. Cutten, R. W. Saunders, and D. T. Llewellyn-Jones, "Theoretical algorithms for satellite-derived sea surface temperatures," J. Geophys. Res. **94,** 3365–3375 (1989).
7. K. A. Van Scoy, K. P. Morris, J. E. Robertson, and A. J. Watson, "Thermal skin effect and the air–sea flux of carbon dioxide: a seasonal high-resolution estimate," Global Biogeochem. Cycles **9,** pp. 253–262 (1995).
8. M. A. Donelan, "Air–sea interaction," in *The Sea: Ocean Engineering Science* (Wiley, New York, 1990).
9. K. Masuda, T. Takashima, and Y. Takayama, "Emissivity of pure and sea waters for the model sea surface in the infrared window regions," Remote Sens. Environ. **24,** 313–329 (1988).
10. P. D. Watts, M. R. Allen, and T. J. Nightingale, "Wind speed effects on sea surface emission and reflection for the along track scanning radiometer," J. Atmos. Ocean. Technol. **13,** 126–141 (1996).
11. P. J. Minnett, R. O. Knuteson, F. A. Best, B. J. Osborne, J. A. Hanafin, and O. B. Brown, "The marine–atmosphere emitted radiance interferometer (M-AERI): a high-accuracy, sea-going infrared spectroradiometer," J. Ocean. Atmos. Technol. **18,** 994–1013 (2001).
12. W. L. Smith, R. O. Knuteson, H. E. Revercomb, W. Feltz, H. B. Howell, W. P. Menzel, N. R. Nalli, O. Brown, J. Brown, P. Minnett, and W. McKeown, "Observations of the infrared radiative properties of the ocean: implications for the measurement of sea surface temperature via satellite remote sensing," Bull. Am. Meteorol. Soc. **77,** 41–52 (1996).
13. J. A. Hanafin, "On properties and characteristics of the sea surface in the infrared," Ph.D. Thesis (University of Miami, Coral Gables, Fla., 2002).
14. L. W. Pinkley, P. P. Sethna, and D. Williams, "Optical constants of water in the infrared: influence of temperature," J. Opt. Soc. Am. **67,** 494–499 (1977).
15. J. E. Bertie and Z. Lan, "Infrared intensities of liquids. XX. The intensity of the OH stretching band of liquid water revisited and the best current values of the optical constants of H_2O (l) at 25C between 15,000 and 1 cm^{-1}," Appl. Spectrosc. **50,** 1047–1057 (1996).
16. L. W. Pinkley and D. Williams, "Optical properties of sea water in the infrared," J. Opt. Soc. Am. **66,** 554–558 (1976).
17. J. Lyman and R. H. Fleming, "Composition of sea water," J. Marine Res. **3,** 134–146 (1940).
18. X. Wu and W. L. Smith, "Emissivity of rough sea surface for 8–13 μm: modeling and verification," Appl. Opt. **36,** 2609–2619 (1997).
19. L. Pontier and C. Dechambenoy, "Determination des constantes optiques de l'eau liquide entre 1 et 40microns. Application au calcul de son pouvoir reflecteur et de son emissivite," Ann. Geophys. **22,** 633–641 (1966).
20. D. J. Segelstein, "The complex refractive index of water," M.Sc. thesis (University of Missouri-Kansas City, Mo., 1981).
21. D. M. Wieliczka, S. Weng, and M. R. Querry, "Wedge shaped cell for highly absorbent liquids: infrared optical constants of water," Appl. Opt. **28,** 1714–1719 (1989).
22. J. A. Shaw, "The effect of instrument polarization sensitivity on sea surface remote sensing with infrared spectroradiometers," J. Atmos. Oceanic Technol. **19,** 820–827 (2002).
23. J. A. Shaw, "Degree of linear polarization in spectral radiances from water-viewing infrared radiometers," Appl. Opt. **38,** 3157–3165 (1999).
24. J. A. Shaw, "Polarimetric measurements of long-wave infrared spectral radiance from water," Appl. Opt. **40,** 5985–5990 (2001).
25. J. W. Salisbury and D. M. D'Aria, "Emissivity of terrestrial materials in the 8–14-μm atmospheric window," Remote Sens. Environ. **42,** 83–106 (1992).
26. C. J. Donlon and T. J. Nightingale, "The effect of atmospheric radiance errors in radiometric sea surface skin temperature measurements," Appl. Opt. **80,** 1656–1661 (2000).
27. C. J. Donlon, S. J. Keogh, D. J. Baldwin, I. S. Robinson, I. Ridley, T. Sheasby, I. J. Barton, E. F. Bradley, T. J. Nightingale, and W. Emergy, "Solid-state radiometer measurements of sea surface skin temperature," J. Atmos. Oceanic Technol. **15,** 775–787 (1998).
28. A. B. Kahle and R. E. Alley, "Separation of temperature and emissance in remotely sensed radiance measurements," Remote Sens. Environ. **42,** 107–111 (1992).
29. C. Cox and W. Munk, "Measurement of the roughness of the sea surface from photographs of the sun's glitter," J. Opt. Soc. Am. **44,** 838–850 (1954).
30. T. Takashima and Y. Takayama, "Emissivity and reflectance of the model sea surface for the use of AVHRR data of NOAA satellites," Papers Meteorol. Geophys. **32,** 267–274 (1981).
31. M. Sidran, "Broadband reflectance and emissivity of specular and rough water surfaces," Appl. Opt. **20,** 3176–3183 (1981).
32. G. M. Hale and M. R. Querry, "Optical constants of water in the 200nm–200 μm wavelength region," Appl. Opt. **12,** 555–563 (1973).
33. D. Friedman, "Infrared characteristics of ocean water (1.5–15 microns)," Appl. Opt. **8,** 2073–2078 (1969).
34. J. A. Shaw and J. H. Churnside, "Scanning laser glint measurements of sea-surface slope statistics," Appl. Opt. **36,** 4202–4213 (1997).